



Published in final edited form as:

ACS Appl Mater Interfaces. 2022 February 23; 14(7): 8718–8727. doi:10.1021/acsami.1c20872.

## Transparent Anti-SARS-CoV-2 and Antibacterial Silver Oxide Coatings

Mohsen Hosseini<sup>1</sup>, Alex W. H. Chin<sup>2,3</sup>, Myra D. Williams<sup>4</sup>, Saeed Behzadinasab<sup>1</sup>, Joseph O. Falkinham III<sup>4</sup>, Leo L. M. Poon<sup>\*,2,3,5</sup>, William A. Ducker<sup>\*,1</sup>

<sup>1</sup>Dept. of Chemical Engineering and Center for Soft Matter and Biological Physics, Virginia Tech, Blacksburg, Virginia, 24061, USA

<sup>2</sup>School of Public Health, LKS Faculty of Medicine, The University of Hong Kong, Hong Kong Special Administrative Region, Hong Kong, China.

<sup>3</sup>Centre for Immunity and Infection, Hong Kong Science Park, Hong Kong, Hong Kong, China

<sup>4</sup>Department of Biological Sciences, Virginia Tech, Blacksburg, Virginia, 24061, USA

<sup>5</sup>HKU-Pasteur Research Pole, LKS Faculty of Medicine, The University of Hong Kong, Hong Kong, China

### Abstract

Transparent antimicrobial coatings can maintain the aesthetic appeal of surfaces or the functionality of a touch screen while adding the benefit of reducing disease transmission. We fabricated an antimicrobial coating of silver oxide particles in a silicate matrix on glass. The matrix was grown by a modified Stöber sol-gel process with vapor-phase water and ammonia. A coating on glass with 2.4 mg of Ag<sub>2</sub>O per mm<sup>2</sup> caused a reduction of 99.3% of SARS-CoV-2, >99.5% of *Pseudomonas aeruginosa*, *Staphylococcus aureus* and methicillin-resistant *Staphylococcus aureus* compared to the uncoated glass after one hour. We envisage that screen protectors with transparent antimicrobial coatings will find particular application to communal

\*Corresponding Authors' Leo Poon llmpoon@hku.hk; William Ducker wducker@vt.edu.

#### Supporting Information

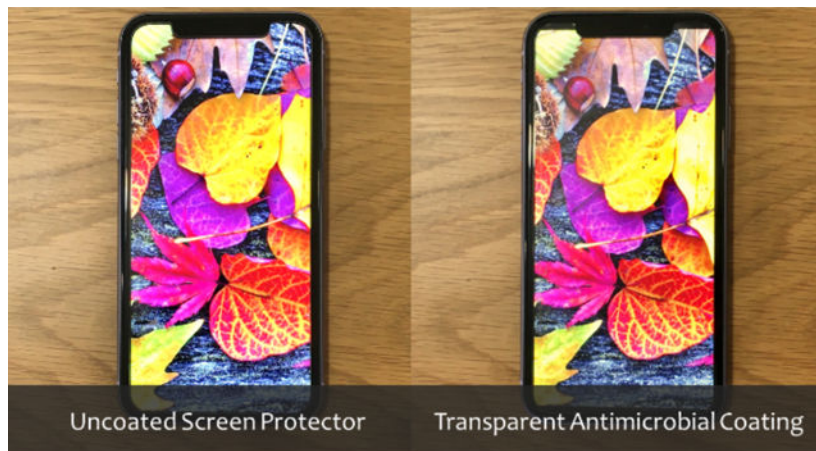
Synthesized particle size distribution (Figure S1). AFM images of 2 × Ag<sub>2</sub>O coating (Figure S2). Surface elemental analysis of coating by EDS (Table S1). SEM images of uncoated glass and TEOS coated glass (Figure S3). Time lapse of sol-gel reaction (Figure S4). The effect of ammonia on the morphology of silver oxide particles (Figure S5). The effect of heat treatment on the morphology of silver oxide particles (Figure S6). Contact angle images of silver oxide coatings (Figure S7). Test of attachment of particles using ultra sonication (Figure S8). The Comparison of SARS-CoV-2 titer Log(TCID<sub>50</sub>/mL) data on TEOS and glass over time (Figure S9). The Comparison of log decrease in *P. aeruginosa* colony forming units on TEOS and glass over time (Figure S10). The Comparison of log decrease in *S. aureus* colony forming units on TEOS and glass over time (Figure S11). The Comparison of log decrease in MRSA colony forming units on TEOS and glass over time (Figure S12). The effect of abrasion in the antibacterial properties of silver oxide coating (Figure S13). Characterization of M – 2 × Ag<sub>2</sub>O-coating (Figure S14). UV-VIS transmission spectrum of uncoated glass and M-2xAg<sub>2</sub>O-coating (Figure S15). The effect of multiple bacteria exposure/sonicating/vortexing/ titration/cleaning on M-2xAg<sub>2</sub>O coating (Figure S16). The effect of absence of light in the antibacterial properties of silver oxide coating (Figure S17). SARS-CoV-2 TCID<sub>50</sub>/mL assay results for Figure 4 (Table S2). *Pseudomonas aeruginosa* CFU assay results for Figure 5 (Table S3). *Staphylococcus aureus* CFU assay results for Figure 5 (Table S4). MRSA CFU assay results for Figure 5 (Table S5). *P. aeruginosa* CFU assay results for Figure 7 (Table S6). MRSA CFU assay results for Figure 7 (Table S7). *P. aeruginosa* CFU assay results for Figure S13 (Table S8). *P. aeruginosa* CFU assays results for Figure S17 (Table S9). MRSA CFU assays results for Figure S17 (Table S10).

#### Conflict of Interest

WD declares part ownership in a startup company that intends to produce surface coatings. Other authors declare no conflict of interest.

touch screens, such as in supermarkets and other check-out or check-in facilities where a number of individuals utilize the same touch screen in a short interval.

## Graphical Abstract



## Keywords

SARS-CoV-2; antibacterial; antiviral; antimicrobial; silver oxide; Ag<sub>2</sub>O; transparent; coating; COVID-19

## 1. Introduction

Pathogenic microbes are responsible for a wide variety of diseases. The routes of transmission vary among microbes and depend on a variety of variables<sup>1</sup> such as temperature and climate. Viruses and microorganisms are known to be transmitted through one or a combination of five main routes:<sup>2</sup> 1) direct contact, 2) airborne, 3) droplet, 4) vehicle-borne including via fomites, and 5) vector-borne. Strategies to reduce pathogen transmission can be used to reduce the prevalence of disease in the community and to reduce healthcare-associated infections (HAIs).

*Staphylococcus aureus* (*S. aureus*), Methicillin-resistant *S. aureus* (MRSA) and *Pseudomonas aeruginosa* (*P. aeruginosa*), three common infectious bacteria<sup>3, 4</sup> in healthcare settings, cause mild to life-threatening infections that set the stage for maladies such as bloodstream, urinary tract and surgical site infections, sepsis and pneumonia<sup>3, 5</sup> These bacteria are considered a major threat to public health<sup>6, 7</sup> and can be transmitted through contaminated fomites.<sup>5, 8, 9</sup>

The Coronavirus disease 2019 (COVID-19) pandemic has dramatically increased the need to control pathogen transfer in different settings. By December 2021, COVID-19 had been responsible for the death of almost more than 5 million people<sup>10</sup> and is known to spread more easily than other corona virus diseases.<sup>11</sup> Although the main transmission route of severe acute respiratory syndrome coronavirus 2 (SARS-CoV-2), the virus that causes COVID-19, is the inhalation of contaminated respiratory droplets,<sup>12</sup> the transmission modes

of this virus are believed to be direct contact, airborne and contaminated fomites.<sup>13</sup> One modelling study suggested that 25% of transmission is via fomites<sup>14</sup> and SARS-CoV-2 is known to be stable on a skin model up to 96 hours at 22 °C.<sup>15</sup>

Hand hygiene is believed to be an effective measure to prevent the microbe transfer through contaminated surface,<sup>16</sup> but in a fomite-rich environment, cleaning of hands would need to be very frequent.<sup>17</sup> Therefore, health professionals suggest a combination of hand hygiene<sup>18</sup> and surface disinfection<sup>19, 20</sup> to mitigate the risk of these microbe transfers.

A parallel approach to the reduction of infection from fomites is to implement coatings on common-use surfaces<sup>21</sup> that quickly inactivate microbes between users. SARS-CoV-2 can remain viable on solid surfaces up to 7 days,<sup>22, 23</sup> and the above mentioned bacteria are stable on surfaces for months,<sup>24, 25</sup> depending on the type of solid and environmental conditions. If these periods were reduced by antimicrobial coatings on common-touch surfaces, then the window of transmission could be shortened and the spread of COVID-19 and other microbial diseases could be reduced.

To this end, coatings have been developed to kill bacteria,<sup>8, 26, 27</sup> or viruses<sup>28</sup> and more recently to inactivate SARS-CoV-2.<sup>29–32</sup> The speed of their action is of great importance; clearly one would like the viability of the surface-adherent microorganisms to be eliminated within minutes or even a shorter time after deposition of the microbe on the solid surface.

Another practical criterion for an antimicrobial coating is retention of the function of the surface after it has been coated. This is our motivation for creating transparent antimicrobial coatings. Transparency is necessary for phone screens, touch screens at supermarkets and check-in facilities, tablets, windows, etc. and touch screens are a known pathway for the spread of pathogens. For example, mobile phones are a major pathway for bacteria spread in hospitals.<sup>33, 34</sup> Touch screens at supermarkets etc., have a series of users in a short time, so it is reasonable that pathogens may be spread by contact at these locations.

The antimicrobial coatings have attracted many researchers in the past few years.<sup>35–38</sup> To date all published work on coatings that inactivate SARS-CoV-2 describe opaque coatings.<sup>29–32</sup> Here we describe a novel transparent silver oxide coating capable of accelerating the inactivation of the virus, SARS-CoV-2, as well as rapidly killing the bacteria *S. aureus*, *P. aeruginosa*. The coating killed both methicillin-tolerant *S. aureus* and methicillin-resistant *S. aureus*. The latter, known as MRSA, is an important public health issue. The antibacterial properties of silver oxide have been previously reported in non-transparent coatings for medical implants<sup>39</sup> and on catheters.<sup>40</sup> No damage, change in morphology or cytotoxic effect has been observed against L929 fibroblast cells<sup>41</sup> or G292 osteoblastic cells,<sup>42</sup> which are mammalian cells. Because of such low cytotoxicity, Ag<sub>2</sub>O can be used in wide variety of applications from tooth paste against dental pathogens<sup>43</sup> to its use in wound healing injections<sup>44</sup>, anticancer carrier drugs for skin cancer<sup>45</sup>, orthopaedic<sup>42</sup> and dental tissue regeneration.<sup>46</sup>

In order to fabricate the transparent coatings we employed a novel binding method based on the Stöber sol-gel process,<sup>47–49</sup> that utilized vapor-phase reactants so that menisci could form and react.<sup>50</sup> Our results indicated that the silver oxide transparent coating caused at

least a 99.8% decrease in SARS-CoV-2, *S. aureus* and *P. aeruginosa* in one hour, and that the resulting coating was transparent and allowed operation of an iPhone touch-screen.

## 2. Materials and Methods

### 2.1 Materials

100% Ethanol (EtOH ACS grade), 70% ethanol (Reagent Grade), sodium hydroxide beads (NaOH ACS grade), nitric acid (70%, ACS grade) and glass slides ( $25 \times 75 \times 1$  mm) were purchased from VWR. Silver nitrate 99.9% and ammonium hydroxide (Certified ACS Plus) were obtained from Fisher Scientific. Tetraethyl orthosilicate 99.999% (TEOS) was purchased from Sigma Aldrich. Deionized (DI) water was from a Milli-Q Reference (MilliporeSigma) water purification system.

### 2.2 Synthesis of Ag<sub>2</sub>O Microparticles

The synthesis of silver oxide particle has been previously described elsewhere.<sup>51, 52</sup> Briefly, 600 mL of 0.01 M AgNO<sub>3</sub> in DI water was stirred while 1200 mL of 0.01 M NH<sub>3</sub> in DI water was added dropwise, and then the mixture was stirred for 10 minutes. Subsequently, 60 mL of 2 M NaOH was added dropwise. The addition of NaOH caused the solution to darken, demonstrating the synthesis of small Ag<sub>2</sub>O particles. The suspension was left for 12 hours, during which time, the particles precipitated. After precipitation, the particles were washed three times with DI water and then three times with ethanol. Lastly, the supernatant liquid was decanted from the particles and particles were left to dry.

### 2.3 Fabrication of Transparent Silver Oxide Coatings

In order to prepare the coating, glass slides were cut into 12×12 mm pieces and cleaned serially with DI water, 70% ethanol, 6 M Nitric acid and DI water respectively. Those glass pieces acted as the Ag<sub>2</sub>O-free, control samples. We prepared two different coatings that differed by the solids-loading of Ag<sub>2</sub>O particles. The Ag<sub>2</sub>O-coating had 5.0 mg/mL Ag<sub>2</sub>O powder in suspension (1.2 mg of Ag<sub>2</sub>O per mm<sup>2</sup> of glass surface) whereas 2 × Ag<sub>2</sub>O-coating had 10 mg/mL Ag<sub>2</sub>O powder in suspension (2.4 mg of Ag<sub>2</sub>O per mm<sup>2</sup>). To prepare the transparent silver oxide-coated surfaces, the glass pieces were O<sub>2</sub> plasma treated at a pressure of less than 200 mTorr and 100 W for 5 minutes. Immediately after the plasma treatment, 34 μL of a suspension of Ag<sub>2</sub>O in 2.8 % (vol/vol) TEOS in ethanol solution was applied on the glass pieces. Substrates were then placed in partially sealed leveled containers to limit evaporation and the self-assembly<sup>53, 54</sup> of the particles accordingly. After two hours, the ethanol was evaporated and samples were transferred to a leveled sealed container in contact with vapors of 8 M DI water in ethanol and 7.62 M ammonia in DI Water for 20 hours. Next, the samples were heat-treated at 50 °C for 40 min. Lastly, samples were blown with high pressure nitrogen, rinsed upside down in DI water for 10 minutes and dried with a nitrogen gas. We used cleaned glass and TEOS samples as controls in antimicrobial experiments.

## 2.4 Characterization of Microparticles and Coatings

The x-ray diffraction (XRD) pattern obtained from a Bruker D8 Advance diffractometer (monochromatic Cu K $\alpha$  x-ray, wavelength=1.5418 Å) was used to identify the structure of the particles. X-ray photoelectron spectroscopy (XPS; PHI VersaProbe III with a monochromatic Al K $\alpha$  source of 1486.6 eV) was employed to assess the chemical composition of the surface of the film. Scanning electron microscopy (JEOL JSM-IT500) and atomic force microscopy (Asylum Research 3D MFP) were utilized to examine the coating morphology and roughness respectively. ImageJ software was employed to obtain the synthesized particle size distribution through SEM images. Surface composition was assessed using electron-dispersive X-ray spectroscopy (Oxford Instruments Ultim Max 100). Optical absorbance and transmittance were measured using an Agilent model 8453 UV-VIS spectrometer. The wettability of the coatings was assessed from the contact angle (First Ten Angstroms FTA125) of 10  $\mu$ L of DI water.

## 2.5 SARS-CoV-2 Assay

We have described the 50% tissue culture infective dose (TCID<sub>50</sub>) method for SARS-CoV-2 viability tests in detail elsewhere.<sup>29, 30</sup> Briefly, both preparation of the virus stock (Hong Kong index SARS-CoV-2 virus) and assessment of cytopathic effect utilized Vero E6 cells. These cells were cultured at 37 °C and 5% CO<sub>2</sub> in 2% fetal bovine serum and 1% v/v penicillin–streptomycin added to Dulbecco’s modified Eagle medium. The viral transport medium consisted of 0.5% (w/v) bovine serum albumin and 0.1% (w/v) glucose in Earle’s balanced salt solution with a pH of 7.4. Control samples and coatings were disinfected with 70% ethanol in water and then dried in air at 37 °C overnight.

The antiviral properties were assessed by placing a 5  $\mu$ L droplet containing 7.8 log unit TCID<sub>50</sub>/mL of SARS-CoV-2 on the test solid at 22–23 °C and 60–70% humidity, and after a predefined time, the sample was eluted in 300  $\mu$ L of viral transport medium. The viable virus was then measured using TCID<sub>50</sub> assay<sup>55, 56</sup> in quadruplicates<sup>57</sup>. Three independently produced solid surfaces were tested for each time point and the antiviral activity at each time point was obtained based on the reduction of log (virus titer).

## 2.6 Antibacterial Assay

**Microbial Strains.**—The microbial strains employed in this study were *P. aeruginosa* strain DSM-9644, *S. aureus* strain ATCC No. 6538, and a methicillin-resistant *S. aureus* (MRSA) strain MA43300 obtained from the Danville Community Hospital (Danville, VA).

**Growth of Microbial Strains.**—Bacterial strains were grown in 5 mL of Tryptic Soy Broth (TSB, BD, Sparks, MD) to mid-exponential phase at 37° C with aeration (60 rpm). Following growth, the purity and identity of the cells in the cultures was verified by streaking bacterial cultures on Tryptic Soy Agar (TSA, BD, Sparks, MD) and incubated at 37° C for 48 hr and examining colonies for species-specific traits (e.g., pigmentation and surface texture).

**Preparation of Microbial Strains for Testing.**—Grown cells were collected by centrifugation (5,000 g for 20 min), the supernatant medium discarded, and the cells

suspended in 5 mL of sterile phosphate-buffered saline (PBS) by vortexing for 60 sec. Those suspensions were centrifuged (5,000 g for 20 min), the supernatant wash discarded, and the washed cells suspended in 5 mL of sterile PBS by vortexing for 60 sec. The number of colony-forming units (CFU)/mL of each washed suspension was measured by spreading 0.10 mL (in duplicate) of serial dilutions in PBS on TSA plates.

**Measurement of Cell Number.**—Cell number of PBS-suspensions of bacteria was measured as colony-forming units (CFU)/mL of suspension. This measures the number of viable cells, i.e., those cells that are able to grow into a colony. A 10-fold dilution series was prepared for each PBS suspension, 0.1 mL of each dilutions was spread on TSA in triplicate, and colonies were counted after 48 hr. incubation at 37° C. If no colonies were present for the least dilution, then we rounded this result up to one colony to enable a log transformation. We set this as the detection limit shown in figures. Any data point at the detection limit is therefore an upper bound for that measurement.

**Measurement of Surface-Killing.**—For each microbial strain, a 10  $\mu$ L droplet of bacterial cells in PBS suspension was placed on each of 3 individual Ag<sub>2</sub>O-coated or uncoated glass pieces. Immediately after drying, each glass piece was transferred to a separate sterile 50 mL centrifuge tube containing 5 mL of sterile PBS, vortexed at the highest setting for 10 sec and sonicated for 1 min. in a Branson Model 12 Ultrasonic Cleaner (Shelton, CT) and the CFU/mL of the suspension measured as described above. The process was repeated at each time point. CFU counts, corrected for dilution, are in tables in the Supporting Information.

## 2.7 Robustness of Coatings

The United States Environmental Protection Agency (EPA) has a required procedure for the evaluation of antibacterial coatings. We followed their procedure<sup>58</sup> but with some minor modifications. The procedure is described more fully in in Supporting Information, but in brief, it consists of repeatedly translating a wet sponge across the coating with a mass of 0.45 kg using a Gardco, Model D10V abrasion 214 tester. The main modification to the EPA procedure was to use ethanol, because our main application was for transparent surfaces, such as electronic displays, that are usually cleaned with alcohol solutions.

We further tested the particle attachment strength by sonicating the coatings for three minutes in ethanol. The absorbance spectra of resulted suspensions were then obtained using UV-VIS to evaluate the detachment of the particles.

## 2.8 Statistics

All experiments were done with three independent trials. Effects were considered significant when  $p$  was near or below 0.05. Linear regression was performed using Excel or MATLAB.



### 3 Results

#### 3.1 Characterization of the Ag<sub>2</sub>O particles

The XRD pattern (Figure 1) of the Ag<sub>2</sub>O particles is consistent with the known cubic space group and the previously-observed XRD pattern of truncated octahedral silver oxide microparticles.<sup>51, 52</sup> SEM images of the particles (Figure 2) show a morphology consistent with the literature.<sup>51, 52</sup> The mean particle size is 1.5 μm (Supporting Information, Figure S1).

#### 3.2 The Coatings Contain Ag<sub>2</sub>O at or near the surface.

Our plan was to have the Ag<sub>2</sub>O protrude from the silica matrix, such that microbes would come into contact with the Ag<sub>2</sub>O surface or dissolved ions. SEM images (Figure 2B–D) are consistent with Ag<sub>2</sub>O protruding from the silica matrix and show a uniform distribution of particles. EDS of individual particles shows a 2.5:1 ratio of Ag:O which is similar to a 2:1 ratio expected for Ag<sub>2</sub>O (Supporting Information, Table S1). We used XPS, which assays only the top 1 nm or so of the interface, to determine whether the Ag<sub>2</sub>O was exposed. The results in Figure 3, which show that the surface has about 9% silver for the Ag<sub>2</sub>O-coating and 19% for the 2 × Ag<sub>2</sub>O-coating, verified that the particles were at or near the surface and that the amount of silver at the surface scaled with the amount added to the coating.

The morphology of the particles changed during film formation: the octahedral shape was transformed into lotus-leaf-type features (Figure 2B–D). These features protrude less than about 2 μm from the surrounding silica layer, which has roughness of about 10 nm (See Figure S2). Silver oxide particles are known to have partial solubility when in contact with ammonia<sup>59</sup> or alkali,<sup>60</sup> and the coating was exposed to ammonia vapor during formation. Therefore, the morphology change is a result of a partial dissolution/precipitation process in the presence of ammonia. Figure S4, S5 and S6 in Supporting information show optical timelapse photography demonstrating that the morphology change is mainly complete after about 12 hours, that ammonia is necessary for the reaction, and that the heat treatment does not affect the Ag<sub>2</sub>O morphology.

The static contact angles for a 10 μL water droplet on Ag<sub>2</sub>O-coating and 2 × Ag<sub>2</sub>O-coating were 62 ± 7° and 67 ± 5°, respectively (See Figure S7 Supporting information). We also examined how firmly the silver particles were attached in the film by exposing the film to ultrasound while immersed in ethanol for 3 minutes. We were not able to detect any particles that were removed by ultrasound (See Figure S8 in Supporting information).

#### 3.3 Silver Oxide Coatings inactivate SARS-CoV-2

The antiviral activity of transparent silver oxide coatings was evaluated by placing a 5 μL droplet containing SARS-CoV-2 on each coating and measuring the viable virus titer at predefined time points. The results in Figure 4 show that silver oxide particles are able to greatly accelerate the decay of SARS-CoV-2 on the Ag<sub>2</sub>O coatings compared to the uncoated solid. There are two reference points for considering the effectiveness of the coatings: (1) comparison to the input microbe titer in the test droplet, which we call “inactivation” and

(2) comparison to the microbe titer on the uncoated glass at the same time, which we call “*Reduction*”, each of which is defined as follows:

$$\log \text{ inactivation} = \text{mean}[\log_{10}(\text{input titer})] - \text{mean}[\log_{10}(\text{sample titer})] \quad (1)$$

$$\log \text{ Reduction} = \text{mean}[\log_{10}(\text{uncoated titer})] - \text{mean}[\log_{10}(\text{coated titer})] \quad (2)$$

$$\% \text{ Inactivation} = \left(1 - 10^{-\log \text{ inactivation}}\right) \times 100 \quad (3)$$

$$\% \text{ Reduction} = \left(1 - 10^{-\log \text{ reduction}}\right) \times 100 \quad (4)$$

In equations (1) and (2) the titers have been made unitless by multiplying by the volume units, so the same volume units must be used for the two means. The TCID<sub>50</sub> assay does not measure numbers of virions and instead, measures the infectious dose of the virus needed to infect 50% of the tissue culture. The experimental reductions and efficiencies are listed in Table 1. ANOVA (with time and Ag<sub>2</sub>O loading as factors) showed that both time ( $p=7 \times 10^{-19}$ ) and concentration of Ag<sub>2</sub>O ( $p=1 \times 10^{-14}$ ) were significant factors affecting the inactivation of SARS-CoV-2.

We observed a very slow inactivation of SARS-CoV-2 titer on the uncoated glass: the TCID<sub>50</sub>/mL was decreased by only 66.7% (0.48 log<sub>10</sub> reduction) after one hour. In contrast, on the Ag<sub>2</sub>O and the 2 × Ag<sub>2</sub>O coatings, the virus was inactivated by 95.4% (1.3 log<sub>10</sub> reduction) and 99.8% (2.6 log<sub>10</sub> reduction) after one hour. When we compared the performance of these two transparent coatings with uncoated glass using (eq 2) and (eq 4), the average *Reduction* was 86.1% for the Ag<sub>2</sub>O-coating and 99.3% for the 2 × Ag<sub>2</sub>O-coating after one hour. The 95% confidence interval (one tailed, heteroscedastic) indicated that the *Reduction* was more than 73.2% on Ag<sub>2</sub>O-coating and more than 95.7% on 2 × Ag<sub>2</sub>O-coating compared to uncoated glass after one hour. The absence of significant *Reduction* for TEOS-only samples confirmed that silver oxide is the active ingredient for inactivating SARS-CoV-2 (Figure S9 Supporting information).

The significance of the silver oxide surface density,  $c$ , and time,  $t$ , can be determined by a regression analysis. For this analysis we included the zero-Ag<sub>2</sub>O (TEOS only) coating, the Ag<sub>2</sub>O-coating and the 2 × Ag<sub>2</sub>O-coating. We included a cross-term ( $tc$ ) because we hypothesized that more SARS-CoV-2 would be inactivated over time if there were a greater density of Ag<sub>2</sub>O in the coating. The regression equation has the following from:

$$\log[\text{TCID}_{50}/\text{mL}] = A - B t - C c - D tc \quad (5)$$

where  $A$ ,  $B$ ,  $C$ , and  $D$  are coefficients to be determined from the regression. A regression analysis using 0 and 1 h data points showed that  $p = 0.12$  for the coefficient of concentration and so this term was deleted and the analysis was rerun with only the  $t$  and  $tc$  terms. For the



cross term,  $Dtc$ ,  $p=4\times 10^{-4}$ , showing that the loss of viral titer depended on the concentration on the surface density. The half-life of the viral titer is:

$$t_{1/2} = \log 2 / (B + Dc) \quad (6)$$

so, the significant value of  $D$  shows that the half-life of SARS-CoV-2 titer decreases with the concentration of  $\text{Ag}_2\text{O}$  in the coating, a major conclusion of this paper. Values of all coefficients are in Table 2.

### 3.4 Silver Oxide Coatings Kill Bacteria

We tested the  $\text{Ag}_2\text{O}$ -coating and the  $2 \times \text{Ag}_2\text{O}$ -coating against three bacteria strains by placing a  $10 \mu\text{L}$  droplet on the solid and measuring the CFU after a predefined period of time. Figure 5 shows the antibacterial activity of silver oxide coatings against *P. aeruginosa*, *S. aureus* and MRSA. Both coatings are extremely effective against all three bacteria as demonstrated by the death of bacteria at 1 h. We quantified the efficacy of the coatings using the following equations:

$$\log \text{ survival} = \text{mean}[\log_{10}(\text{sample CFU})] - \text{mean}[\log_{10}(\text{input CFU})] \quad (7)$$

$$\log \text{ Reduction} = \text{mean}[\log_{10}(\text{uncoated CFU})] - \text{mean}[\log_{10}(\text{coated CFU})] \quad (8)$$

$$\% \text{ Killing} = (1 - 10^{\log \text{ survival}}) \times 100 \quad (9)$$

$$\% \text{ Reduction} = (1 - 10^{-\log \text{ reduction}}) \times 100 \quad (10)$$

We use the word survival for simplicity but acknowledge that the CFU assay measures those cells that can reproduce to form a colony. Table 2 lists the survival (in log units) compared to both the input of bacteria, and the *Reduction* compared to glass at one hour. Both coatings demonstrated excellent antibacterial activity and the results indicate that the number of viable bacteria was reduced by at least 1.8 log units (>98.7% *Reduction*) on the  $\text{Ag}_2\text{O}$ -coating and at least 2 log units (>99.3% *Reduction*) on the  $2 \times \text{Ag}_2\text{O}$ -coating compared to glass in 1 hour. Again, the *Reduction* was greater with more  $\text{Ag}_2\text{O}$  present in the film, and there was no significant *Reduction* for TEOS-only coatings (See Figure S10, S11 and S12 in Supporting Information), indicating that  $\text{Ag}_2\text{O}$  is the active ingredient.

The significance of time and  $\text{Ag}_2\text{O}$  concentration was again determined by a regression analysis using Equation 5 (by replacing  $\text{TCID}_{50}$  with CFU). Again, the effect of concentration was insignificant and was omitted in subsequent analysis. In common with SARS-CoV-2, the cross term,  $tc$ , shows that a greater density of  $\text{Ag}_2\text{O}$  in the coating leads to greater inactivation of all three bacteria over time. More precisely, a greater density of  $\text{Ag}_2\text{O}$  in the coating reduces the half-life of the bacteria.

The  $2 \times \text{Ag}_2\text{O}$ -coating demonstrated an excellent bacterial activity by reducing the viable cells of *P. aeruginosa* and MRSA by more than 99.9% ( $p=7 \times 10^{-6}$  and  $p=7 \times 10^{-3}$  respectively) after one hour, and reducing *S. aureus* by 99.5% ( $p=2 \times 10^{-7}$ ) after one hour compared to uncoated glass. The  $\text{Ag}_2\text{O}$ -coating also showed a considerable *Reduction* in comparison to uncoated glass. The *Reduction* of viable *P. aeruginosa*, *S. aureus* and MRSA on this coating was 99.9% ( $p=7 \times 10^{-6}$ ), 98.3% ( $p=6 \times 10^{-6}$ ) and 96.4% ( $p=4 \times 10^{-4}$ ) respectively compared to uncoated glass after one hour (Figure 5).

### 3.5 $\text{Ag}_2\text{O}$ -coatings are Transparent and Retain Touch-Screen Function.

The  $\text{Ag}_2\text{O}$ -coatings are transparent, with about 60–75% of the transmission of glass in the visible range, and only small variation in transmission with color (Figure 6A). As a result, the colors of a smart phone screen are retained when a screen protector with the  $2 \times \text{Ag}_2\text{O}$ -coating is attached to a smart phone screen (Figure 6B). Importantly, the screen function is retained with the coating in place (See Video in Supporting Information).

### 3.6 The Antimicrobial Coatings are Resistant to Abrasion

We also conducted an EPA abrasion test (slightly modified) on the  $2 \times \text{Ag}_2\text{O}$  coating. After abrasion, the antimicrobial properties were unchanged, demonstrating that the coating was robust (See Figure S13 in Supporting Information).

### 3.7 Efficacy after Repeated Exposure to Droplets containing Bacterial Suspension

Although  $2 \times \text{Ag}_2\text{O}$  coating is very robust against water and ethanol and passes the modified EPA abrasion test, the antibacterial efficacy was diminished after multiple exposures to suspensions of bacteria in droplets. Therefore, we modified the fabrication method to obtain a more robust coating. The principal change was that we increased the amount of silica in the film by increasing the TEOS from 2.8% to 20 % (vol/vol) in ethanol solution. To achieve polymerization of the greater thickness of coating, we increased the time of exposure to the vapor to 60 h and the heat treatment to 75 °C for 40 min. We refer to this modified coating as M –  $2 \times \text{Ag}_2\text{O}$ -coating. The M –  $2 \times \text{Ag}_2\text{O}$ -coating was characterized with SEM with XPS (Figure S14), which showed a lower silver content, consistent with some of the silver oxide being covered by the thicker TEOS layer. The visible spectrum showed that the transparency of  $2 \times \text{Ag}_2\text{O}$ -coating was retained (Figure S15).

We tested the antibacterial performance of M –  $2 \times \text{Ag}_2\text{O}$ -coating against *P. aeruginosa* and MRSA (figure 7). After 1 h, the microbial survival was below the detection limit with > 99.99% killing, a 99.80% *Reduction* for *P. aeruginosa* and 99.97% *Reduction* for MRSA compared to the uncoated glass. The results were not statistically different from the  $2 \times \text{Ag}_2\text{O}$ -coating at any time point. We then determined the efficacy of this coating after multiple exposure to the microbe, with a series of exposure/bacterial assay/cleaning cycles (See the Supporting Information **for details**). More than 99.9% of *P. aeruginosa* were killed in 1 h after four cycles (See Figure S16 in Supporting Information). These results show the coating is still highly active after repeated exposure to the bacteria.

## 4 Discussion

### 4.1 Antimicrobial Mechanism of Silver Oxide

The strong antibacterial activity<sup>61–63</sup> of silver oxide has been attributed to silver ion species,<sup>64–66</sup> which have a finite solubility in water ( $\text{Ag}_2\text{O} + \text{H}_2\text{O} \leftrightarrow 2\text{Ag}^+ + 2\text{OH}^-$ ,  $\text{pK}_s = 7.7$ ;  $\text{Ag}_2\text{O} + \text{H}_2\text{O} \leftrightarrow 2\text{Ag}(\text{OH})$ ,  $\text{pK}_s = 5.7$ ;  $\text{Ag}_2\text{O} + \text{H}_2\text{O} + 2\text{OH}^- \leftrightarrow 2\text{Ag}(\text{OH})_2^-$ ,  $\text{pK}_s = 3.7$ ).<sup>67</sup> The mechanism of action of silver ions is believed to be either one or a combination of 1) the generation of reactive oxygen species (ROS)<sup>64</sup> and exertion of oxidative stress on cells, and 2) the release and penetration of  $\text{Ag}^+$  ions into the microbe and damaging the cell membrane.<sup>65, 66</sup> Park et al reported that the superoxide radical was the major form of the reactive oxygen species generated by silver ions, while  $\text{H}_2\text{O}_2$  was unlikely to be induced.<sup>68</sup> These reactive oxygen species exert an oxidative stress and damage DNA accordingly which will lead to the killing of bacteria.<sup>69</sup> Silver ions, on the other hand, lead to loss of cell viability by damaging the cell membrane.<sup>66</sup> Minoshima et al. reported that silver oxide particles damage the viral envelope of influenza A virus and bacteriophage Q $\beta$  virus.<sup>70</sup>

There is a possibility that the efficacy of  $\text{Ag}_2\text{O}$  depends on light. If the bandgap of the particles were in the visible range, light could cause the excitation of electron to the conduction band, which could then act as reducing agents. We compared the antimicrobial efficacy of  $2 \times \text{Ag}_2\text{O}$  coating in visible light and in the dark. (See Figure S17 in Supporting Information). A student's t-test did not resolve a significant difference between light and dark measurements ( $p > 0.05$ ) and, therefore, the silver oxide coating does not require light for its antimicrobial properties.

## 5 Conclusion

We fabricated two silver oxide in silica coatings,  $\text{Ag}_2\text{O}$  and  $2 \times \text{Ag}_2\text{O}$ , that inactivate SARS-CoV-2 (95.4% and 99.8% in one hour) and kill *P. aeruginosa*, (99.99% in 1 h), *S. aureus* (99.78% and 99.93% in 1h), including the antibiotic-resistant strain, MRSA (99.33% and 99.98% in 1h). The coating was fabricated using a modification of the Stöber method to bind silver oxide particles to a glass substrate. The coated glass is transparent, which means that it does not degrade the aesthetic appeal of materials and it can be applied where transparency is important for function. For example, we showed that when a mobile phone screen was coated, both the screen clarity and the function of the touch-screen was retained. The combination of transparency and antimicrobial action means that the coating should find application for multi-user touchscreens, such as in check-out facilities in grocery stores.

## Supplementary Material

Refer to Web version on PubMed Central for supplementary material.

## Acknowledgements

The authors thank Stephen McCartney for assisting in capturing a part of SEM images and acknowledge use of Electron Microscopy facilities and x-ray diffraction machine within the Nanoscale Characterization and Fabrication Laboratory and Material Characterization Laboratory at Virginia Polytechnic Institute and state university. We also thank Xu Feng for capturing the XPS spectra and acknowledge the use of Surface Analysis Laboratory in

Department of Chemistry at Virginia Tech, which is supported by the National Science Foundation under Grant No. CHE-1531834. This work was supported by the National Science Foundation under Grant No. CBET-1902364, the Health and Medical Research Fund (COVID190116), and the National Institute of Allergy and Infectious Diseases (contract HHSN272201400006C).

## References

- (1). Andersen BM Microbes, Transmission Routes and Survival Outside the Body. In Prevention and Control of Infections in Hospitals, Springer, 2019; pp 23–28.
- (2). Antonovics J; Wilson AJ; Forbes MR; Hauffe HC; Kallio ER; Leggett HC; Longdon B; Okamura B; Sait SM; Webster JP The Evolution of Transmission Mode. *Philosophical Transactions of the Royal Society B: Biological Sciences* 2017, 372 (1719), 20160083.
- (3). Weiner LM; Webb AK; Limbago B; Dudeck MA; Patel J; Kallen AJ; Edwards JR; Sievert DM Antimicrobial-resistant Pathogens Associated with Healthcare-associated Infections: Summary of Data Reported to the National Healthcare Safety Network at the Centers for Disease Control and Prevention, 2011–2014. *infection control & hospital epidemiology* 2016, 37 (11), 1288–1301. [PubMed: 27573805]
- (4). Solberg CO Spread of Staphylococcus aureus in Hospitals: Causes and Prevention. *Scandinavian journal of infectious diseases* 2000, 32 (6), 587–595. [PubMed: 11200366]
- (5). Xiao S; Jones RM; Zhao P; Li Y. The Dynamic Fomite Transmission of Methicillin-resistant Staphylococcus aureus in Hospitals and the Possible Improved Intervention Methods. *Building and Environment* 2019, 161, 106246.
- (6). Davis KA; Stewart JJ; Crouch HK; Florez CE; Hospenthal DR Methicillin-resistant Staphylococcus aureus (MRSA) Nares Colonization at Hospital Admission and Its Effect on Subsequent MRSA Infection. *Clinical Infectious Diseases* 2004, 39 (6), 776–782. [PubMed: 15472807]
- (7). Harris SR; Feil EJ; Holden MT; Quail MA; Nickerson EK; Chantratita N; Gardete S; Tavares A; Day N; Lindsay JA Evolution of MRSA During Hospital Transmission and Intercontinental Spread. *Science* 2010, 327 (5964), 469–474. [PubMed: 20093474]
- (8). Page K; Wilson M; Parkin IP Antimicrobial Surfaces and Their Potential in Reducing the Role of the Inanimate Environment in the Incidence of Hospital-acquired Infections. *Journal of materials chemistry* 2009, 19 (23), 3819–3831.
- (9). Desai R; Pannaraj PS; Agopian J; Sugar CA; Liu GY; Miller LG Survival and Transmission of Community-Associated Methicillin-resistant Staphylococcus aureus from Fomites. *American journal of infection control* 2011, 39 (3), 219–225. [PubMed: 21458684]
- (10). COVID-19 Dashboard by the Center for Systems Science and Engineering (CSSE) at Johns Hopkins University (JHU). Johns Hopkins University, 2020. <https://coronavirus.jhu.edu/map.html> (accessed December 27, 2021).
- (11). Coutard B; Valle C; de Lamballerie X; Canard B; Seidah N; Decroly E. The Spike Glycoprotein of The New Coronavirus 2019-nCoV Contains A Furin-Like Cleavage Site Absent in Cov of The Same Clade. *Antiviral research* 2020, 176, 104742.
- (12). Prather KA; Wang CC; Schooley RT Reducing Transmission of SARS-CoV-2. *Science* 2020, 368 (6498), 1422–1424. [PubMed: 32461212]
- (13). Sia SF; Yan L-M; Chin AW; Fung K; Choy K-T; Wong AY; Kaewpreedee P; Perera RA; Poon LL; Nicholls JM Pathogenesis and Transmission of SARS-CoV-2 in Golden Hamsters. *Nature* 2020, 583 (7818), 834–838. [PubMed: 32408338]
- (14). Meiksin A. Dynamics of COVID-19 Transmission Including Indirect Transmission Mechanisms: A Mathematical Analysis. *Epidemiology & Infection* 2020, 148, e257. [PubMed: 33092672]
- (15). Harbourt DE; Haddow AD; Piper AE; Bloomfield H; Kearney BJ; Fetterer D; Gibson K; Minogue T. Modeling the Stability of Severe Acute Respiratory Syndrome Coronavirus 2 (SARS-CoV-2) on Skin, Currency, and Clothing. *PLoS neglected tropical diseases* 2020, 14 (11), e0008831.
- (16). Cromer AL; Latham SC; Bryant KG; Hutsell S; Gansauer L; Bendyk HA; Steed R; Carney MC Monitoring and Feedback of Hand Hygiene Compliance and the Impact on Facility-acquired

- Methicillin-resistant *Staphylococcus aureus*. *American journal of infection control* 2008, 36 (9), 672–677. [PubMed: 18834733]
- (17). Bhalla A; Pultz NJ; Gries DM; Ray AJ; Eckstein EC; Aron DC; Donskey CJ Acquisition of Nosocomial Pathogens on Hands After Contact with Environmental Surfaces Near Hospitalized Patients. *Infection Control & Hospital Epidemiology* 2004, 25 (2), 164–167. [PubMed: 14994944]
  - (18). Lei H; Xiao S; Cowling BJ; Li Y. Hand Hygiene and Surface Cleaning Should Be Paired for Prevention of Fomite Transmission. *Indoor Air* 2020, 30 (1), 49–59. [PubMed: 31545534]
  - (19). Lei H; Jones RM; Li Y. Exploring Surface Cleaning Strategies in Hospital to Prevent Contact Transmission of Methicillin-resistant *Staphylococcus aureus*. *BMC infectious diseases* 2017, 17 (1), 1–9. [PubMed: 28049444]
  - (20). Monge FA; Jagadesan P; Bondu V; Donabedian PL; Ista L; Chi EY; Schanze KS; Whitten DG; Kell AM Highly Effective Inactivation of SARS-CoV-2 by Conjugated Polymers and Oligomers. *ACS Appl. Mater. Interfaces* 2020, 12 (50), 55688–55695. [PubMed: 33267577]
  - (21). Hosseini M; Behzadinasab S; Benmamoun Z; Ducker WA The Viability of SARS-COV-2 on Solid Surfaces. *Curr. Opin. Colloid Interface Sci* 2021, 101481.
  - (22). Van Doremalen N; Bushmaker T; Morris DH; Holbrook MG; Gamble A; Williamson BN; Tamin A; Harcourt JL; Thornburg NJ; Gerber SI Aerosol and Surface Stability of SARS-CoV-2 as Compared with SARS-CoV-1. *New England Journal of Medicine* 2020, 382 (16), 1564–1567. [PubMed: 32182409]
  - (23). Chin AW; Chu JT; Perera MR; Hui KP; Yen H-L; Chan MC; Peiris M; Poon LL Stability of SARS-CoV-2 in Different Environmental Conditions. *The Lancet Microbe* 2020, 1 (4), e146. [PubMed: 33521712]
  - (24). Kramer A; Schwebke I; Kampf G. How long do nosocomial pathogens persist on inanimate surfaces? A systematic review. *BMC infectious diseases* 2006, 6 (1), 1–8. [PubMed: 16390553]
  - (25). Williams C; Davis DL Methicillin-resistant *Staphylococcus aureus* fomite survival. *American Society for Clinical Laboratory Science* 2009, 22 (1), 34–38.
  - (26). Yuan W; Ji J; Fu J; Shen J. A Facile Method to Construct Hybrid Multilayered Films as A Strong and Multifunctional Antibacterial Coating. *Journal of Biomedical Materials Research Part B: Applied Biomaterials* 2008, 85 (2), 556–563. [PubMed: 18098202]
  - (27). Heidenau F; Mittelmeier W; Detsch R; Haenle M; Stenzel F; Ziegler G; Gollwitzer H. A Novel Antibacterial Titania Coating: Metal Ion Toxicity and in Vitro Surface Colonization. *Journal of Materials Science: Materials in Medicine* 2005, 16 (10), 883–888. [PubMed: 16167096]
  - (28). Rakowska PD; Tiddia M; Faruqui N; Bankier C; Pei Y; Pollard AJ; Zhang J; Gilmore IS Antiviral Surfaces and Coatings and Their Mechanisms of Action. *Commun. Mat* 2021, 2 (1), 1–19.
  - (29). Behzadinasab S; Chin A; Hosseini M; Poon LL; Ducker WA A Surface Coating that Rapidly Inactivates SARS-CoV-2. *ACS Appl. Mater. Interfaces* 2020, 12 (31), 34723–34727. [PubMed: 32657566]
  - (30). Hosseini M; Chin AW; Behzadinasab S; Poon LL; Ducker WA Cupric Oxide Coating That Rapidly Reduces Infection by SARS-CoV-2 via Solids. *ACS Appl. Mater. Interfaces* 2021, 13 (5), 5919–5928. [PubMed: 33480246]
  - (31). Hutasoit N; Kennedy B; Hamilton S; Luttick A; Rashid RAR; Palanisamy S. SARS-CoV-2 (COVID-19) Inactivation Capability of Copper-Coated Touch Surface Fabricated by Cold-Spray Technology. *Manufacturing Letters* 2020, 25, 93–97. [PubMed: 32904558]
  - (32). Hosseini M; Behzadinasab S; Chin AW; Poon LL; Ducker WA Reduction of Infectivity of SARS-CoV-2 by Zinc Oxide Coatings. *ACS Biomaterials Science & Engineering* 2021, 7 (11), 5022–5027. [PubMed: 34613703]
  - (33). Olsen M; Campos M; Lohning A; Jones P; Legget J; Bannach-Brown A; McKirdy S; Alghafri R; Tajouri L. Mobile Phones Represent A Pathway for Microbial Transmission: A Scoping Review. *Travel medicine and infectious disease* 2020, 101704.
  - (34). Karabay O; Koçoglu E; Tahtaci M. The Role of Mobile Phones in the Spread of Bacteria Associated with Nosocomial Infections. *J Infect Dev Ctries* 2007, 1 (1), 72–73.
  - (35). Deussenberg C; Wang Y; Shukla A. Recent Innovations in Bacterial Infection Detection and Treatment. *ACS Infectious Diseases* 2021, 7 (4), 695–720. [PubMed: 33733747]

- (36). Alkekha D; Hammond PT; Shukla A. Layer-by-layer Biomaterials for Drug Delivery. Annual review of biomedical engineering 2020, 22, 1–24.
- (37). Salwiczek M; Qu Y; Gardiner J; Strugnell RA; Lithgow T; McLean KM; Thissen H. Emerging Rules for Effective Antimicrobial Coatings. Trends in Biotechnology 2014, 32 (2), 82–90. [PubMed: 24176168]
- (38). Cloutier M; Mantovani D; Rosei F. Antibacterial Coatings: Challenges, Perspectives, and Opportunities. Trends in biotechnology 2015, 33 (11), 637–652. [PubMed: 26463723]
- (39). Akiyama T; Miyamoto H; Yonekura Y; Tsukamoto M; Ando Y; Noda I; Sonohata M; Mawatari M. Silver Oxide-containing Hydroxyapatite Coating Has in vivo Antibacterial Activity in the Rat Tibia. Journal of Orthopaedic Research 2013, 31 (8), 1195–1200. [PubMed: 23589130]
- (40). Johnson JR; Roberts PL; Olsen RJ; Moyer KA; Stamm WE Prevention of Catheter-associated Urinary Tract Infection with A Silver Oxide-coated Urinary Catheter: Clinical and Microbiologic Correlates. Journal of Infectious Diseases 1990, 162 (5), 1145–1150. [PubMed: 2230239]
- (41). Babu PJ; Doble M; Raichur AM Silver Oxide Nanoparticles Embedded Silk Fibroin Spuns: Microwave Mediated Preparation, Characterization and Their Synergistic Wound Healing and Antibacterial Activity. Journal of colloid and interface science 2018, 513, 62–71. [PubMed: 29132106]
- (42). Shahrbabak MSN; Sharifianjazi F; Rahban D; Salimi A. A Comparative Investigation on Bioactivity and Antibacterial Properties of Sol-gel Derived 58S Bioactive Glass Substituted by Ag and Zn. Silicon 2019, 11 (6), 2741–2751.
- (43). Manikandan V; Velmurugan P; Park J-H; Chang W-S; Park Y-J; Jayanthi P; Cho M; Oh B-T Green Synthesis of Silver Oxide Nanoparticles and Its Antibacterial Activity Against Dental Pathogens. 3 Biotech 2017, 7 (1), 72.
- (44). Kim MH; Park H; Nam HC; Park SR; Jung J-Y; Park WH Injectable Methylcellulose Hydrogel Containing Silver Oxide Nanoparticles for Burn Wound Healing. Carbohydrate polymers 2018, 181, 579–586. [PubMed: 29254010]
- (45). Fakhri A; Tahami S; Nejad PA Preparation and Characterization of Fe<sub>3</sub>O<sub>4</sub>-Ag<sub>2</sub>O Quantum Dots Decorated Cellulose Nanofibers as A Carrier of Anticancer Drugs for Skin Cancer. Journal of Photochemistry and Photobiology B: Biology 2017, 175, 83–88. [PubMed: 28865318]
- (46). Vu AA; Robertson SF; Ke D; Bandyopadhyay A; Bose S. Mechanical and Biological Properties of ZnO, SiO<sub>2</sub>, and Ag<sub>2</sub>O Doped Plasma Sprayed Hydroxyapatite Coating for Orthopaedic and Dental Applications. Acta biomaterialia 2019, 92, 325–335. [PubMed: 31082568]
- (47). Hench LL; West JK The Sol-gel Process. Chemical reviews 1990, 90 (1), 33–72.
- (48). Ghimire PP; Jaroniec M. Renaissance of Stöber Method for Synthesis of Colloidal Particles: New Developments and Opportunities. Journal of Colloid and Interface Science 2020, 584, 838–865. [PubMed: 33127050]
- (49). Stöber W; Fink A; Bohn E. Controlled Growth of Monodisperse Silica Spheres in The Micron Size Range. Journal of colloid and interface science 1968, 26 (1), 62–69.
- (50). Chang Y-R; Taylor S; Duncan S; Mazilu DA; Ritter A; Ducker WA Fabrication of Stabilized Colloidal Crystal Monolayers. Colloids and Surfaces A: Physicochemical and Engineering Aspects 2017, 514, 185–191.
- (51). Chen Y-J; Chiang Y-W; Huang MH Synthesis of Diverse Ag<sub>2</sub>O Crystals and Their Facet-Dependent Photocatalytic Activity Examination. ACS Appl. Mater. Interfaces 2016, 8 (30), 19672–19679. [PubMed: 27411371]
- (52). Wang X; Wu H-F; Kuang Q; Huang R-B; Xie Z-X; Zheng L-S Shape-dependent Antibacterial Activities of Ag<sub>2</sub>O Polyhedral Particles. Langmuir 2010, 26 (4), 2774–2778. [PubMed: 20141212]
- (53). Rabani E; Reichman DR; Geissler PL; Brus LE Drying-mediated Self-assembly of Nanoparticles. Nature 2003, 426 (6964), 271–274. [PubMed: 14628047]
- (54). Grosso D; Cagnol F; Soler-Illia G. d. A.; Crepaldi EL; Amenitsch H; Brunet-Bruneau A; Bourgeois A; Sanchez C. Fundamentals of Mesostructuring Through Evaporation-induced Self-assembly. Advanced Functional Materials 2004, 14 (4), 309–322.



- (55). Malenovska H. Virus Quantitation by Transmission Electron Microscopy, TCID50, and the Role of Timing Virus Harvesting: A Case Study of Three Animal Viruses. *J. Virol. Methods* 2013, 191 (2), 136–140. [PubMed: 23603437]
- (56). Chan K; Lai S; Poon L; Guan Y; Yuen K; Peiris J. Analytical Sensitivity of Rapid Influenza Antigen Detection Tests for Swine-origin Influenza Virus (H1N1). *J. Clin. Virol* 2009, 45 (3), 205–207. [PubMed: 19539521]
- (57). Reed LJ; Muench H. A Simple Method of Estimating Fifty Percent Endpoints. *American Journal of Epidemiology* 1938, 27 (3), 493–497.
- (58). Interim Method for Evaluating the Efficacy of Antimicrobial Surface Coatings. EPA. 10/2/2020. <https://www.epa.gov/pesticide-analytical-methods/antimicrobial-testing-methods-procedures-interim-method-evaluating> (accessed August 25, 2021).
- (59). Britton H; Williams WG Electrometric Studies of The Precipitation of Hydroxides. Part XIII. The Constitution of Aqueous Solutions of Silver Oxide in Ammonia, mono-, di-, and tri-methylamine and-ethylamine, Pyridine And Ethylenediamine; with A Note on the Dissociation Constants of The Amines. *Journal of the Chemical Society (Resumed)* 1935, 796–801.
- (60). Johnston HL; Cuta F; Garrett AB The Solubility of Silver Oxide in Water, in Alkali And in Alkaline Salt Solutions. The Amphoteric Character of Silver Hydroxide. *Journal of the American Chemical Society* 1933, 55 (6), 2311–2325.
- (61). Allahverdiyev AM; Abamor ES; Bagirova M; Rafailovich M. Antimicrobial Effects of TiO<sub>2</sub> And Ag<sub>2</sub>O Nanoparticles Against Drug-resistant Bacteria and Leishmania Parasites. *Future microbiology* 2011, 6 (8), 933–940. [PubMed: 21861623]
- (62). Negi H; Saravanan PR; Agarwal T; Zaidi MGH; Goel R. In Vitro Assessment of Ag<sub>2</sub>O Nanoparticles Toxicity Against Gram-positive and Gram-negative Bacteria. *The Journal of general and applied microbiology* 2013, 59 (1), 83–88. [PubMed: 23518522]
- (63). Rokade AA; Patil MP; Yoo SI; Lee WK; Park SS Pure Green Chemical Approach for Synthesis of Ag<sub>2</sub>O Nanoparticles. *Green Chemistry Letters and Reviews* 2016, 9 (4), 216–222.
- (64). Rajabi A; Ghazali MJ; Mahmoudi E; Baghdadi AH; Mohammad AW; Mustafah NM; Ohnmar H; Naicker AS Synthesis, Characterization, and Antibacterial Activity of Ag<sub>2</sub>O-loaded Polyethylene Terephthalate Fabric via Ultrasonic Method. *Nanomaterials* 2019, 9 (3), 450. [PubMed: 30889785]
- (65). Bellantone M; Williams HD; Hench LL Broad-spectrum Bactericidal Activity of Ag<sub>2</sub>O-doped Bioactive Glass. *Antimicrobial agents and chemotherapy* 2002, 46 (6), 1940–1945. [PubMed: 12019112]
- (66). Li D; Chen S; Zhang K; Gao N; Zhang M; Albasher G; Shi J; Wang C. The Interaction of Ag<sub>2</sub>O Nanoparticles with *Escherichia coli*: Inhibition–sterilization Process. *Scientific reports* 2021, 11 (1), 1–9. [PubMed: 33414495]
- (67). Feitknecht W; Schindler P. Solubility Constants of Metal Oxides, Metal Hydroxides and Metal Hydroxide Salts in Aqueous Solution. *Pure and Applied Chemistry* 1963, 6 (2), 125–206.
- (68). Park H-J; Kim JY; Kim J; Lee J-H; Hahn J-S; Gu MB; Yoon J. Silver-ion-mediated Reactive Oxygen Species Generation Affecting Bactericidal Activity. *Water research* 2009, 43 (4), 1027–1032. [PubMed: 19073336]
- (69). Makvandi P; Wang C. y.; Zare EN; Borzacchiello A; Niu L. n.; Tay R. Metal-based Nanomaterials in Biomedical Applications: Antimicrobial Activity and Cytotoxicity Aspects. *Advanced Functional Materials* 2020, 30 (22), 1910021.
- (70). Minoshima M; Lu Y; Kimura T; Nakano R; Ishiguro H; Kubota Y; Hashimoto K; Sunada K. Comparison of The Antiviral Effect of Solid-State Copper and Silver Compounds. *Journal of hazardous materials* 2016, 312, 1–7. [PubMed: 27015373]

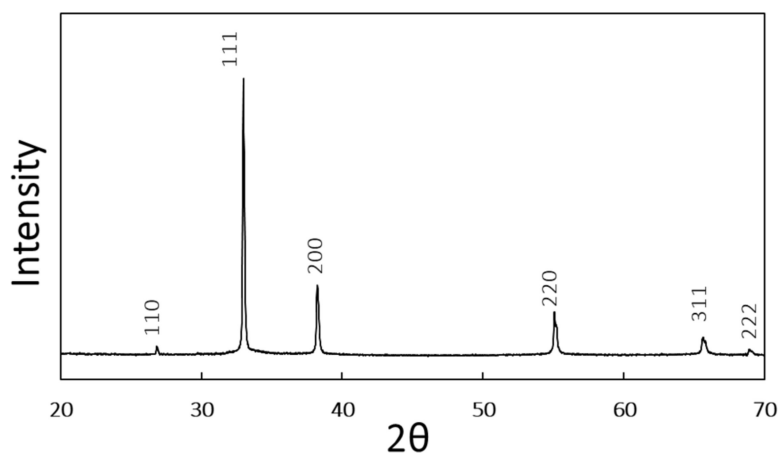


**Figure 1.** XRD pattern of the  $\text{Ag}_2\text{O}$  particles, which is consistent with the known pattern of  $\text{Ag}_2\text{O}$  microparticles.<sup>51, 52</sup> The numbers on each peak indicate the Miller Indices of the scattering planes.

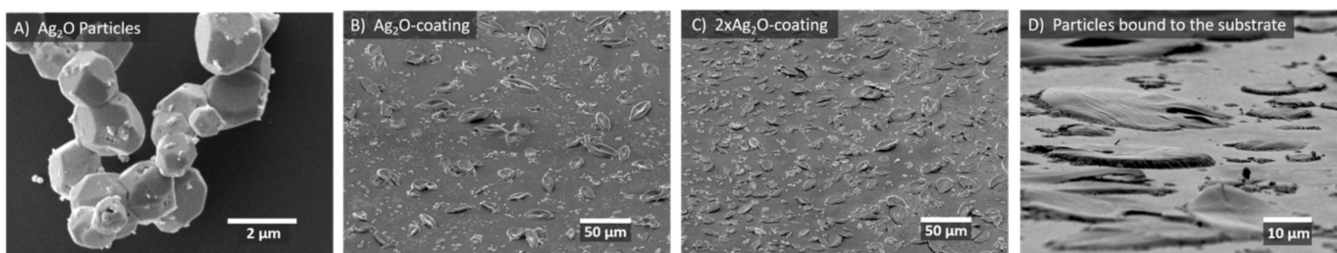


**Figure 2.** SEM images of A) Ag<sub>2</sub>O particles prior to fabrication of the coating. B) Ag<sub>2</sub>O-coating C) 2 × Ag<sub>2</sub>O-coating and D) Tilted and magnified view of C. The SEM images show that the coating of particles is uniform and is consistent with Ag<sub>2</sub>O protruding from the silica matrix. Additional SEM images of controls are included in the Supporting Information, Figure S3.

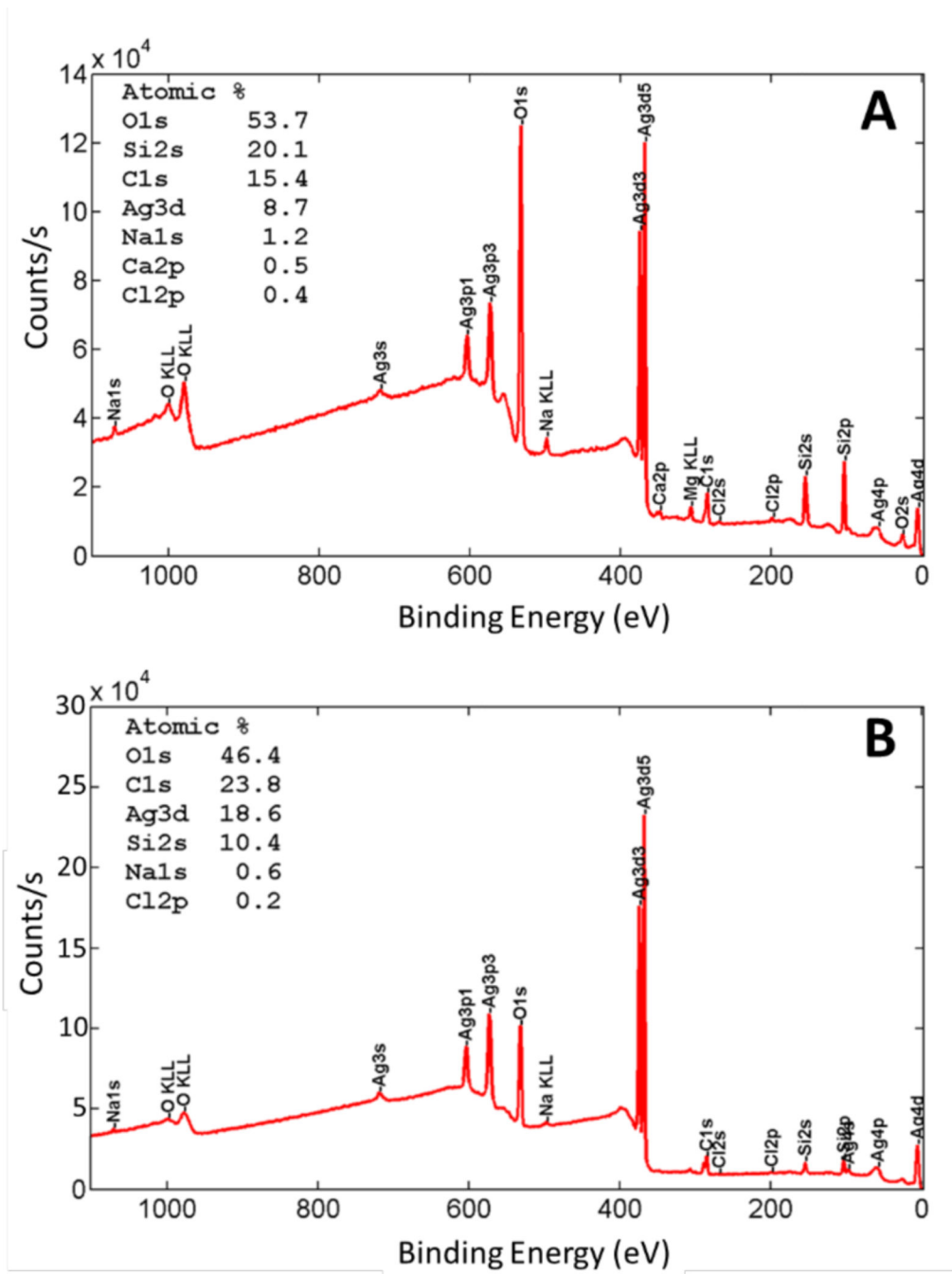


**Figure 3.** XPS of the silver oxide coatings showing the elemental analysis and confirming presence of silver and oxygen on the surface. A) Survey spectrum of Ag<sub>2</sub>O-coating and B) Survey spectrum 2 × Ag<sub>2</sub>O-coating.

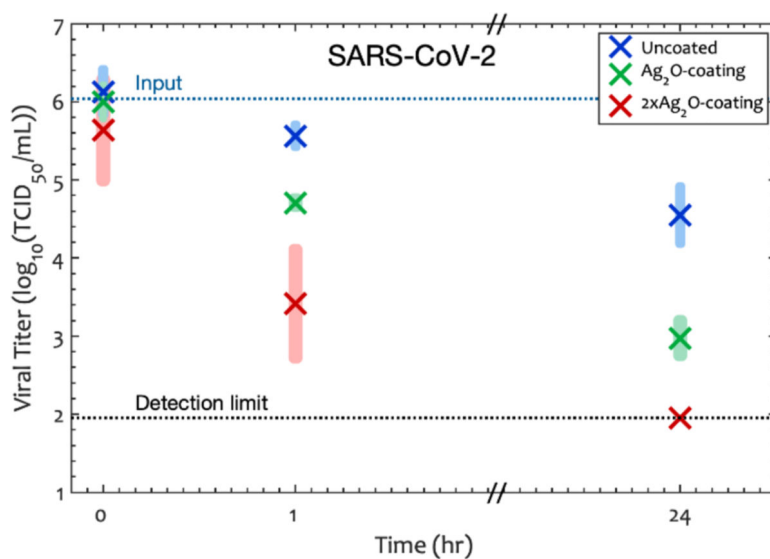


**Figure 4.** SARS-CoV-2 titer as a function of time and Ag<sub>2</sub>O surface density in the coating. Ag<sub>2</sub>O-coating has 1.18 mg of Ag<sub>2</sub>O per mm<sup>2</sup> of glass surface whereas 2 × Ag<sub>2</sub>O-coating has 3.6 mg of Ag<sub>2</sub>O per mm<sup>2</sup>. Shaded rectangles represent the 95% confidence interval calculated only for the points at that condition, and × represents the average of the log of the viral titer at each time point. The results show that the coating inactivates the SARS-CoV-2 virus.

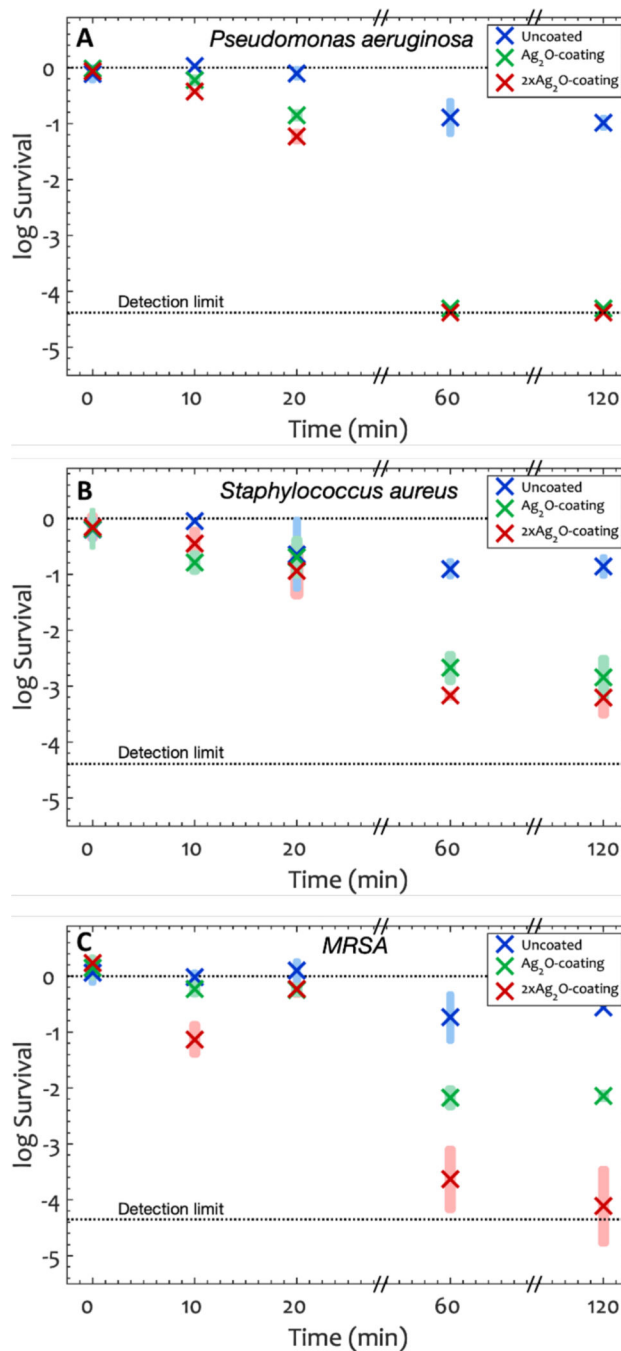


**Figure 5.** Log survival in Colony forming units (Equation 1) over time for A) *P. aeruginosa*, B) *S. aureus* and C) MRSA. Shaded rectangles represent the 95% confidence interval and × represents the average of the log of the CFU at each time point. The log input titers were 6.08, 6.09 and 6.05 for *P. aeruginosa*, *S. aureus* and MRSA respectively. After one hour, the average killing percentage of *P. aeruginosa*, *S. aureus* and MRSA were >99.9% on 2 × Ag<sub>2</sub>O-coating and >99.3% on Ag<sub>2</sub>O-coating. Silver oxide transparent coatings



significantly reduced the CFU units of the bacteria compared to uncoated glass (ANOVA  $p=7\times 10^{-3}$ ).

Author Manuscript

Author Manuscript

Author Manuscript

Author Manuscript

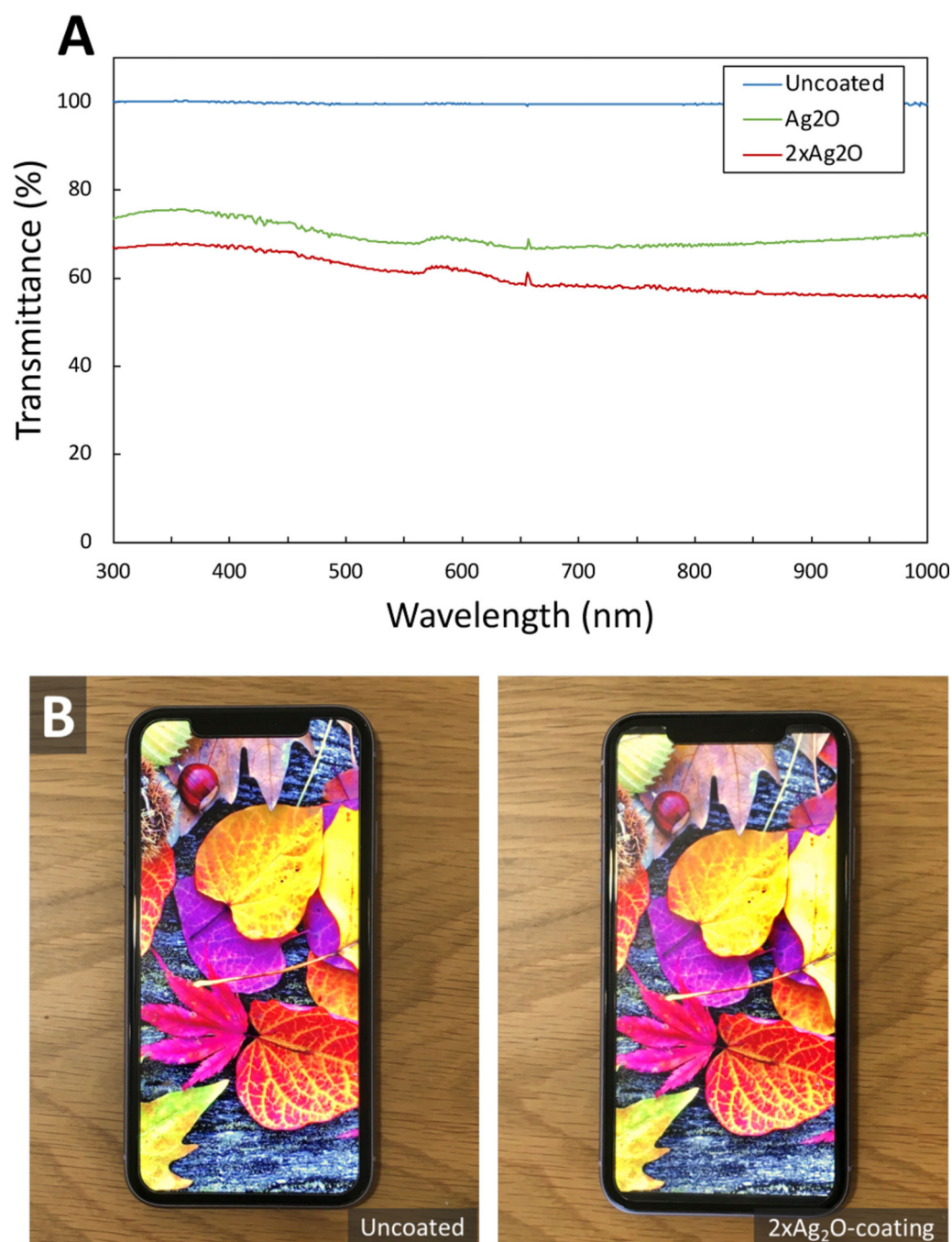


**Figure 6.**

A) UV-VIS transmission spectrum of glass, Ag<sub>2</sub>O-coating and 2 × Ag<sub>2</sub>O-coating showing that both films demonstrate more than 60–75% transparency in the visible range (400–700 nm)  
B) A smart phone (iPhone 11) with uncoated and 2 × Ag<sub>2</sub>O-coated screen protector (Mkeke, Amazon B07HRN9J19, tempered glass). The visual appeal and the touch screen function are retained with the antimicrobial screen protector in place.

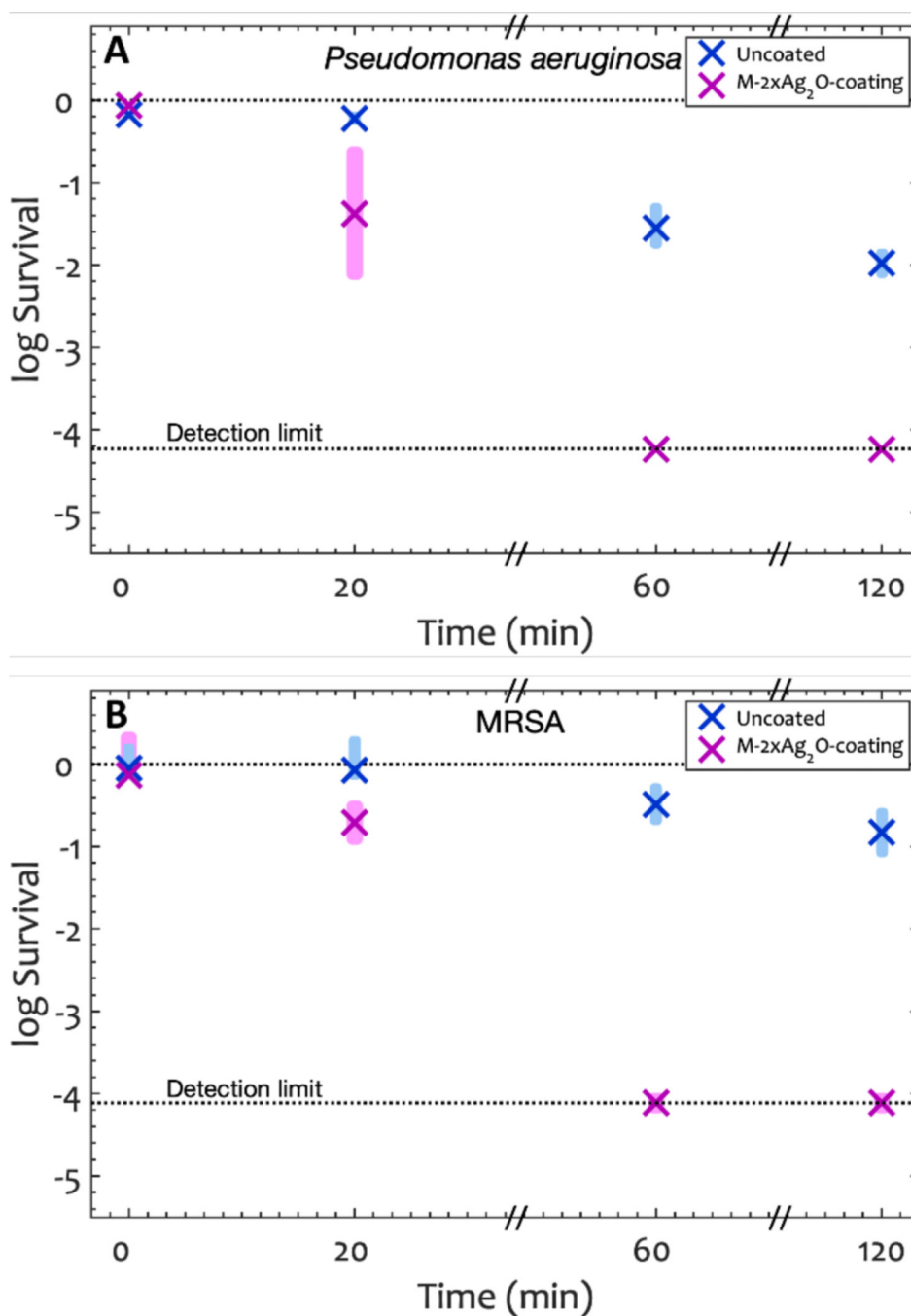


**Figure 7.** Log Survival in Colony forming units (Equation 6) over time for A) *P. aeruginosa*, and B) MRSA on M – 2 × Ag<sub>2</sub>O-coating. Shaded rectangles represent the 95% confidence interval and × represents the average of the log of the CFU at each time point. The log input titers were 5.93±0.02 for *P. aeruginosa* and 6.05±0.12 for MRSA. After one hour, the average killing percentage of *P. aeruginosa* and MRSA were 99.99% on M – 2 × Ag<sub>2</sub>O-coating.

The antibacterial results on M – 2 × Ag<sub>2</sub>O-coating are not statistically different from the 2 × Ag<sub>2</sub>O-coating results (two tailed, unpaired  $p>0.12$ ).

Author Manuscript

Author Manuscript

Author Manuscript

Author Manuscript

**Table 1.**

log Inactivation, log survival, and log reduction of microbes after 1 hour. Inactivation and killing compare to the droplet suspension at the that was used to inoculate the solid and *Reduction* compares to glass at the same time point.

Coating	SARS-CoV-2		<i>P. aeruginosa</i>		<i>S. aureus</i>		MRSA	
	Inactivation	Reduction	Survival	Reduction	Survival	Reduction	Survival	Reduction
Ag <sub>2</sub> O	1.34	0.86	-4.68	3.79	-2.67	1.77	-2.18	1.44
2 × Ag <sub>2</sub> O	2.62	2.15	-4.68	3.79	-3.16	2.26	-3.63	2.89

Author Manuscript

Author Manuscript

Author Manuscript

Author Manuscript

**Table 2.**

Linear regression coefficients for Equation 5. *C* was omitted because it was not significant in any microorganism. The small *p* values for *D* show that the half-life of all the microorganisms decreases with concentration of silver oxide in the coating. The linear regression was run with *t* in units of hours and *c* is in units of mg/mm<sup>2</sup>. For SARS-CoV-2, only the 0h and 1 h data was included because all the data for the 2 × Ag<sub>2</sub>O beyond 1 h was below the detection limit, so only the upper bound was known.

variable	coefficient	SARS-CoV-2		<i>P. aeruginosa</i>		<i>S. aureus</i>		MRSA	
		value	<i>p</i>	value	<i>p</i>	value	<i>p</i>	value	<i>p</i>
constant	<i>A</i>	5.904	3×10 <sup>-18</sup>	5.835	10-15	5.709	10-19	6.048	10-20
<i>t</i>	<i>B</i>	0.243	0.28	0.014	0.07	0.008	0.07	0.006	0.16
<i>t · c</i>	<i>D</i>	0.923	1×10 <sup>-6</sup>	0.018	1.9×10 <sup>-4</sup>	0.011	2.3×10 <sup>-4</sup>	0.015	3.5×10 <sup>-6</sup>